Seismic landslide susceptibility assessment based on seismic ground motion and earthquake disaster analysis

Ailan Che[1], Hanxu Zhou[1], Jinchang Chen[1], Yuchen Wu[1], Ziyao Xu[1]

[1] School of Naval Architecture, Ocean and Civil Engineering, Shanghai Jiao Tong University, 800 Dongchuan Road, Shanghai 200240, China.
alche@sjtu.edu.cn

Abstract. Seismic motion is one of the significant factors triggering slope instability. Landslides induced by intense earthquakes pose a great threat on the public security and traffic safety. About 720 landslides were caused by the 2014 Ms6.5 Ludian earthquake. The seismic ground motion records of Ludian earthquake and the influencing factors of seismic landslides are analyzed, and the susceptibility of landslides was evaluated in combination with machine learning models (BP neural network and SVM). The characteristics of Ludian earthquake motion records in time domain, frequency domain and time-frequency domain reveal that, the maximum value of PGA reached 949.2cm/s^2 (EW), and the duration of seismic wave within the nearest station to epicenter was 5.0s (EW), 4.9s (NS) and 4.3s (UD), respectively. The result of Hilbert Huang Transform suggests that large instantaneous and cumulative energy concentrated in low frequency region (0-5 Hz), which can be considered to be related to large area landslides. Twelve factors are selected as the influencing factors of seismic landslides under Ludian earthquake, and the spatial correlation analysis indicates that the relation between factors and seismic landslide is characterized by strong nonlinear properties, of which ground motion parameters show a strong positive correlation with landslide distribution. The receiver operating characteristic (ROC) curve is adopted to compare the performance of two models. The results show that the AUC values of two curves are 90.1% and 89.5%, respectively, showing that BP neural network has higher accuracy of seismic landslide susceptibility results, and illustrating dependency on spatial distribution of seismic ground motion parameters.

Keywords: Ludian Earthquake, Seismic landslides, Hilbert Huang Transform, BP neural network, Support Vector Machine, Landslide susceptibility.

1 Introduction

Earthquake is a main factor inducing landslides. The statistical data show that earthquakes with magnitude greater than 4.0 could induce landslides [1], and the seismic disasters would be severe under earthquakes with magnitude above 6.0. For example, the Mw 6.7 Northridge earthquake in the United States in 1994 induced more than 11000 landslides in an area of nearly 10000 km^2 [2]. The Mw 6.9 Iwate

Miyagi inland earthquake in Japan in 2008 produced 4161 landslides, including 3779 shallow mudslides [3-4]. Approximately 56000 landslides and collapses were triggered by Ms 8.0 Wenchuan earthquake in China in 2008, which directly led to nearly 30000 deaths, accounting for about 1/3 of the total number of earthquake deaths [5-9]. The M_w 6.6 Hokkaido earthquake in 2018 produced about 3000 landslides and 41 people died in the earthquake, of which 36 were caused by large-scale landslide [10]. Therefore, it is of great significance to realize landslides susceptibility assessment, which could provide reference for emergency rescue work and post-earthquake reconstruction.

With the development of seismic monitoring instruments, data transmission and processing technology, it has gradually become a reality to quickly calculate the seismic parameters and evaluate the seismic intensity according to the seismic ground motions. After the Kanto earthquake in 1923, in order to solve the problem of seismic resistance of buildings, it was proposed to develop strong motion observation instruments. In 1932, the United States first deployed a strong seismograph, and the strong motion records of the Long Beach earthquake in California were obtained in the same year. In 1940, the first record with PGA (peak ground acceleration) > 0.3g (El Centro) was obtained [11]. Strong motion observation in China started in 1962, Xin-feng River dam construction. Since 2000, strong motion observation in China has developed rapidly [12]. Based on the strong motion data, the source location, source depth and magnitude can be determined, and seismic intensity could be evaluated rapidly. The rapid evaluation of seismic intensity can be carried out through the empirical statistical model, based on the attenuation law or on the quantitative relationship between seismic intensity and ground motion parameters [13].

The seismic disasters are closely related to the characteristics of seismic ground motion. Many cases show that moderate magnitude earthquake can cause large scale disasters and the disasters induced by the earthquakes with close magnitude present completely different characteristics, which are closely related to the characteristics of seismic ground motions and local site effect. For example, a Mw 5.6 earthquake occurred at Ionian offshore, which caused the high-level seismic hazard and huge disasters in Sicily (Italy) [14]. Two large earthquakes (Ms 6.6 Jinggu Earthquake and the Ms 6.5 Ludian Earthquake) occurred in Yunnan province, China in 2014. The magnitude of the two earthquakes is close and local site conditions are similar, but the disasters have a big difference. Large landslides and buildings with 3 and more floors are destroyed in Ludian earthquake, however, few landslides or damaged structures were induced by Jinggu earthquake [15]. Seismic landslides depend on the frequency components and peak ground acceleration of input ground motions [16-21]. In theory, high frequency seismic ground motion with shorter wave-length than dimensions of slopes unlikely trigger landslides because high frequency seismic wave drive different parts of slope in the opposite direction simultaneously, so, the whole slope would remain stable. On the other hand, low frequency seismic wave with longer wavelength than dimensions of slopes can lead slope move in the same direction, which more likely induce landslides [22-23]. Similar with landslides, damage characteristics of structures also closely related to the input seismic ground motions. The pulse-like ground motions can increase the inelastic displacement demand of SDOF (single de-

grees of freedom) systems, especially when the ratio of normalized shaking period T to velocity pulse period Tp is less than one [24-25]. So, it is need to consider the characteristics of ground motion in seismic landslide susceptibility evaluation.

Seismic landslide susceptibility evaluation initially focused on the mechanism of landslides, then statistical models and machine learning methods are implemented with the development of computer science. According to whether a mechanical model with definite physical meaning is established during the assessment, landslide susceptibility evaluation methods can be divided into two categories: deterministic method and non-deterministic method. Deterministic method includes slope limit equilibrium analysis, numerical simulation, Newmark permanent displacement method, etc. The Newmark model is the most widely used deterministic method, which calculates the displacement of the slope to decide whether the slope is stable [26]. However, it requires detailed geological data and spatial parameters as support. So, when the model is applied in region, assumptions and simplifications are made which makes the result less accurate [27]. And many methods have been developed to solve this problem such as building an integrated Spectral Element Method (SEM)-Newmark model [28], combing non-deterministic model with Newmark method [29-30] and so on. Among non-deterministic methods, mathematical and statistical models are used to explore the characteristics of data and make decisions on landslide susceptibility. Support vector Machine model (SVM) is a binary model, which has good applicability for imprecise and small sample size problems [31-32]. Artificial neural network (ANN) model is also a widely used model in landslide susceptibility [33]. Except for the basic neural network model, many improvements have been made to obtain higher evaluation accuracy [34-35]. Recently, with the developing of study, many scholars begin to combine different methods for better application [36-37]. Also, various models are implemented in the same area to compare the accuracy of evaluation result for a better understanding of model performance [38-40].

This work investigated the amplitude, duration and spectrum (in time and time-frequency domains) of typical seismic ground motion in Ludian earthquake at first. Then, the characteristics of seismic disasters and the conditioning factors of disaster were analyzed. Considering the characteristics mentioned above, seismic landslide susceptibility evaluation based on machine learning method (BP neural network and SVM) were performed at last. This work has practical significance for major infrastructure construction and disaster prevention and reduction planning.

2 Seismic ground motion and disaster characteristics in Ludian earthquake

Earthquake frequently occur in the Yunnan Province, China. Since the detailed earthquake records, 23.6% of the earthquakes with M $\geqslant$ 7.0 occurred in Yunnan Province, which accounts for only 4.1% of the land area of China. From 1949 to 2020, there were 8 strong earthquakes with M $\geqslant$ 7.0 in Yunnan Province. Recent strong earthquakes in Yunnan Province include Ludian Ms 6.5 earthquake in 2014, Jinggu Ms 6.6 earthquake in 2014, Yingjiang Ms 6.1 earthquake in 2014 and Yangbi

Ms 6.4 earthquake in 2021. Among them, Ludian earthquake caused the largest disasters and casualties. The epicenter intensity of Ludian earthquake up to IX and the focal depth is approximately 12 km, which killed 617 people, injured 2400 and destroyed 86000 buildings. In this section, we mainly introduced the typical strong motion in amplitude, duration and spectrum at first. Then, disaster characteristics and the possible influencing factors of it were analyzed.

2.1 Seismic ground motion characteristics

The distribution of intensity map is shown in Fig 1. Within the intensity map, 7 strong motion stations were triggered, including 1 in the IX region, 1 in VII region and 5 in VI region. The basic information of each station was shown in Table 1. Two of them (HYC and QJT) at rock site. 53LLT with 8.3 km epicentral distance and 53HZH with epicentral distance 65.9 km are the nearest and farthest stations from the epicenter respectively.

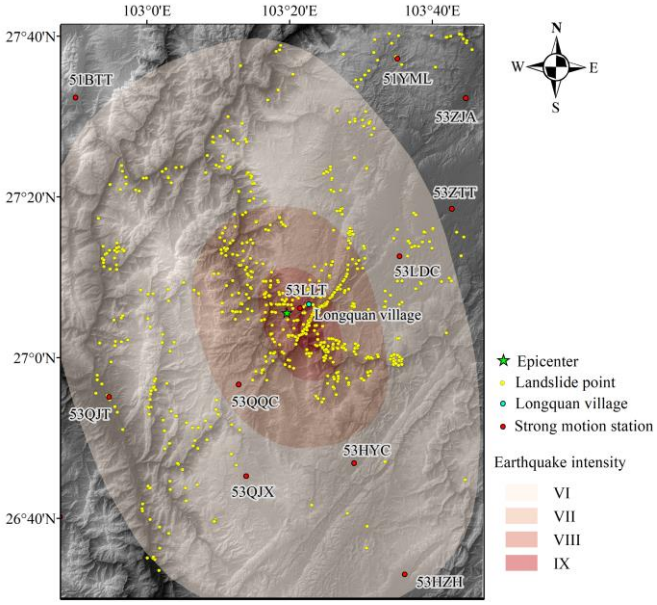

Fig. 1. Intensity map and seismic landslide inventory map in Ludian earthquake

The specific wave forms of 53LLT in three directions are shown in Fig. 2(a). The whole length of time is approximately 130s. The PGA (peak ground motion) in three directions is 949.2cm/s^2 (EW), 705.8cm/s^2 (NS) and 504.4cm/s^2 (UD), respectively. PGA shows a decreasing trend with the increase of epicentral distance, but it is not linear decreasing especially in 53QJX, where PGA has a great increase, as shown in Fig. 2(b). So, the PGA decays relatively slowly.

Table 1. Strong motion stations in Ludian earthquake (within the intensity map)

Event	Stations	Site conditions	Epicentral distance (km)	Intensity scale	PGA (cm/s^2)		
					EW	NS	UD
Ludian earthquake	53LLT	soil	8.3	IX	949.2	705.8	504.4
	53QQC	soil	18.7	VII	146.0	140.3	52.8
	53LDC	soil	32.5	VI	45.9	44.8	25.6
	53QJX	soil	38.1	VI	135.2	133.4	65.0
	53HYC	rock	39.6	VI	88.3	87.7	47.5
	53QJT	rock	46.4	VI	24.8	20.6	-13.2
	53HZH	soil	65.9	VI	50.2	69.2	16.0

The duration of seismic ground motion can reflect the cumulative effect of earthquake on the stability of slope or structures. The duration includes absolute duration and relative duration. We used Kawashinat bracketed duration to reflect the effect, which is a kind of relative duration. It takes the duration between the first and last two times reaching or exceeding a fraction (1/5 ~ 1/2) of the PGA as the duration. It is taken 0.3 in this work. The duration of each seismic ground motion is listed in Table 2. 53LLT has the shortest duration compared with other motions, which are 5.0 (EW), 4.9 (NS) and 4.3 (UD). With the increase of epicentral distance, the duration shows an increasing trend. It reflects that the 53LLT motion has a large and instantaneous inertia force to the slope or structures.

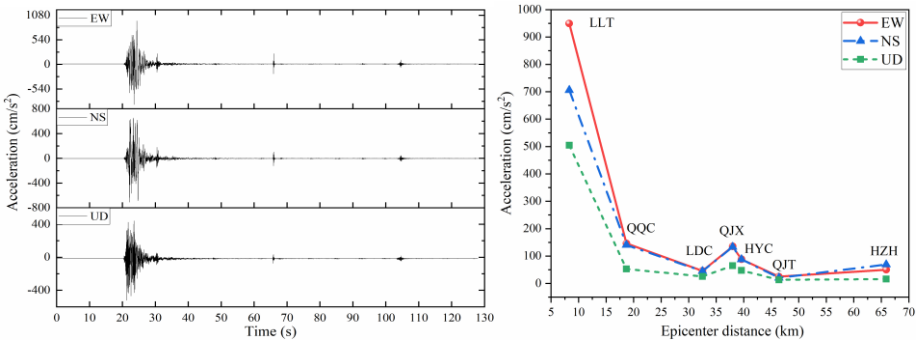

(a) Acceleration time history (b) Attenuation law of PGA

Fig. 2. Acceleration time history of 53LLT and attenuation law of PGA

Table 2. Duration of acceleration time history (within the intensity map)

Events	Station	Duration (s)		
		EW	NS	UD
Ludian earthquake	53LLT	5.0	4.9	4.3
	53QQC	11.4	12.1	14.4
	53LDC	11.5	15.3	15.2
	53QJX	13.3	10.1	13.4
	53HYC	12.1	12.1	9.0
	53QJT	16.6	20.3	21.3
	53HZH	6.8	4.2	16.7

In order to clarify the frequency characteristics of the motions, FFT (Fast Fourier Transform) was done and the Fourier spectrum was obtained. Fourier spectrums of 53LLT in three directions are shown in Fig. 3. It shows that the energy (amplitude) is concentrated within 35Hz. Three predominate frequency in EW and NS directions are same, which are within 0-5Hz, 5-10Hz and 10-15Hz respectively. The first predominate frequency (0-5Hz) is clear than other predominate frequency. The distribution of predominate frequency in UD direction is different from EW and NS directions. Three predominate frequency are within 0-5Hz, 5-15Hz and 15-20Hz and the second predominate frequency is the most outstanding.

The time-frequency characteristics of motions are investigated by Hilbert spectrum in the study. In order to acquire the spectrum, the original signal was decomposed into series of intrinsic mode function (IMF) by Variational Mode Decomposition (VMD) at first, because the original signal does not meet the conditions of Hilbert transform. Each IMF is well behaved in Hilbert transform. The Hilbert spectrum is acquired by composing the spectrum of each IMF. Hilbert spectrums of 53LLT in three directions are shown in Fig. 4. Hilbert spectrum reflects the distribution characteristics of instantaneous energy. Instantaneous energy mainly distributed at 20-30s. The shape of the spectrum presents multi peaks. The energy in EW and NS directions mainly distributed within three frequency range which are 0-5Hz, 5-10Hz and 10-15Hz. Peak instantaneous energy is in 0-5Hz. Compared with EW and NS directions, the frequency range of main instantaneous energy in UD directions has a slight increase and the peak energy is lived in the second and third predominate frequency.

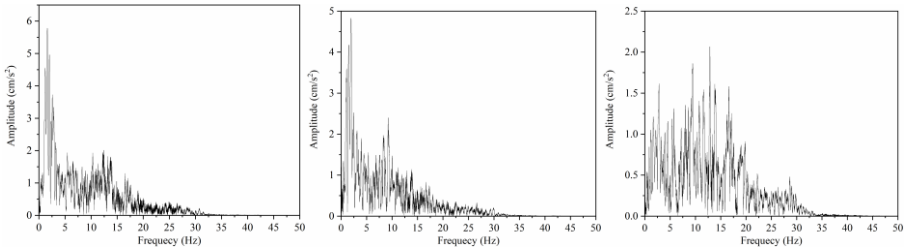

(a) EW (b) NS (c) UD

Fig. 3. Fourier spectrums of 53LLT in three directions

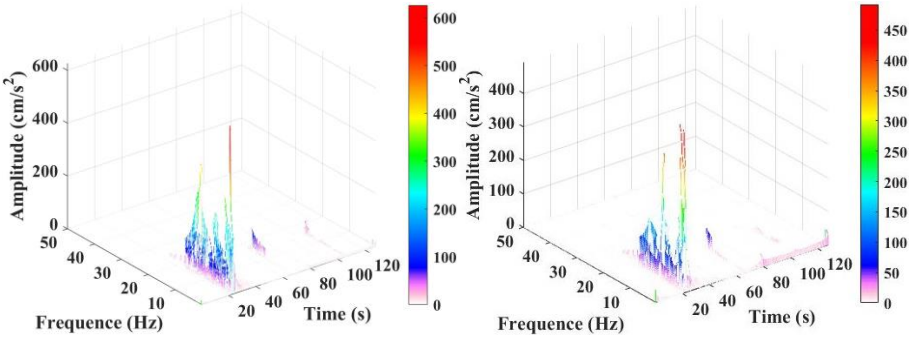

(a) EW (b) NS

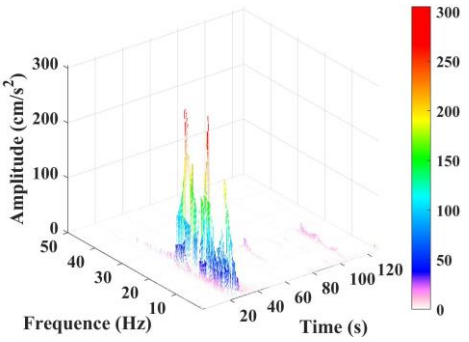

(c) UD

Fig. 4. Hilbert spectrums of 53LLT in three directions

Marginal spectrum is the integral of Hilbert spectrum over time. It reflects the distribution characteristics of cumulative energy at different frequencies. Marginal spectrums of 53LLT in three directions are shown in Fig. 5. The shape of marginal spectrums is close to the Fourier spectrum, however, the predominate frequency shown in marginal spectrum is clearer than Fourier spectrum. Three predominate frequencies in EW direction are 1.625Hz, 6.625Hz and 12.625Hz. Three predominate frequencies in NS direction are same to that in EW direction. In UD direction, predominate frequencies are 3.125Hz, 10.125Hz and 16.625Hz, and the peak energy occurs at the second frequency.

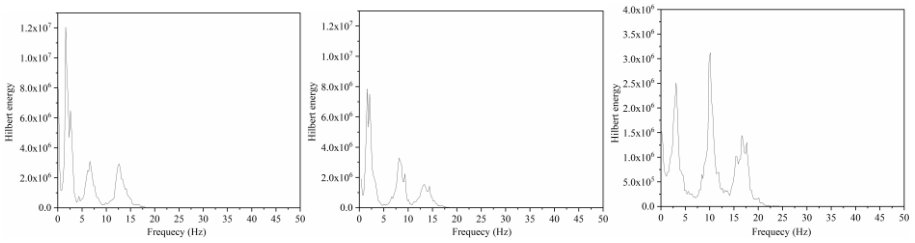

(a) EW (b) NS (c) UD

Fig. 5. Marginal spectrums of 53LLT in three directions

Above results show that the ground motion of 53LLT has large PGA, short duration, large instantaneous and cumulative energy concentrated in low frequency region (0-5Hz), and decay of PGA is relatively slow, which caused the huge disasters including large landslides and seriously destroyed building in local area.

2.2 Factor analysis of seismic landslides

Seismic landslides have the characteristics of wide influence area, complex formation mechanism and various influencing factors. In order to evaluate the susceptibility of seismic landslides, it is quite essential to analyze the condition factors related to the landslide first.

The landslide inventory of Ludian earthquake was mapped based on the data recorded during field investigation. A total number of 714 seismic landslides are compiled, as show in Fig. 1. In presented study, 12 conditioning factors of Ludian earthquake are considered to explore the relationship between factors and the susceptibility of seismic landslides. Among these factors, the internal factors contain elevation, slope, slope aspect, surface curvature, profile curvature, distance to fault, distance to river, NDVI, and lithology. The external factors consist of PGA, PGV and epicenter distance.

To evaluate the landslide sensitivity of each causative factor, frequency ratio method is implemented. The frequency ratio can be calculated by the following formula：

$$\mathrm{FR} = \frac{N_i/A_i}{N/A}$$

Where: for each factor *k*, FR is the frequency ratio of class *i* of factor *k*, *Ni* is the number of landslides within class *i*, and *Ai* is the area of class *i*, *N* is the total number of landslides, and *A* is the total area of the study area. It can be seen that the larger the ration of frequency is, the higher the landslide sensitivity of the factor is. This method excludes the influence of the class area itself on the assessment of relationship between landslide and each factor.

The frequency ratios of each class of 12 factors are calculated and the results are shown in Fig. 6. For the internal factors, Fig. 6(a) reveals that landslides are concentrated in the area with an elevation of about 1400-1800m, there is no single positive correlation between landslide sensitivity and elevation. And Fig. 6(b) reflects probability of landslide increases with the increasement of slope degree. The class of 65-70 degree has the highest landslide sensitivity. As can be seen from Fig. 6(f, g), the landslide sensitivity of fault distance and river distance decreases monotonically with the increase of distance on the whole. The landslide sensitivity of river distance within 3 km and fault distance within 4 km are the highest. Fig. 6(h) shows that the sensitivity of NDVI to landslide is similar in all sections, and the sensitivity is most prominent when the value ranges from 0.09 to 0.12. Lithology is also in strong relation with landslides, and landslides are often concentrated in specific strata. It can be seen from the Fig. 6(i) that the Ordovician and Devonian strata are significantly more sensitive to landslides than other strata. As for seismic parameters, the rule is more obvious. Co-seismic landslides are strongly correlated with PGA and PGV. Fig. 6(j, k, l) indicate that in general, the landslide sensitivity shows a good relationship with the increase of PGA and PGV and the decrease of epicenter distance.

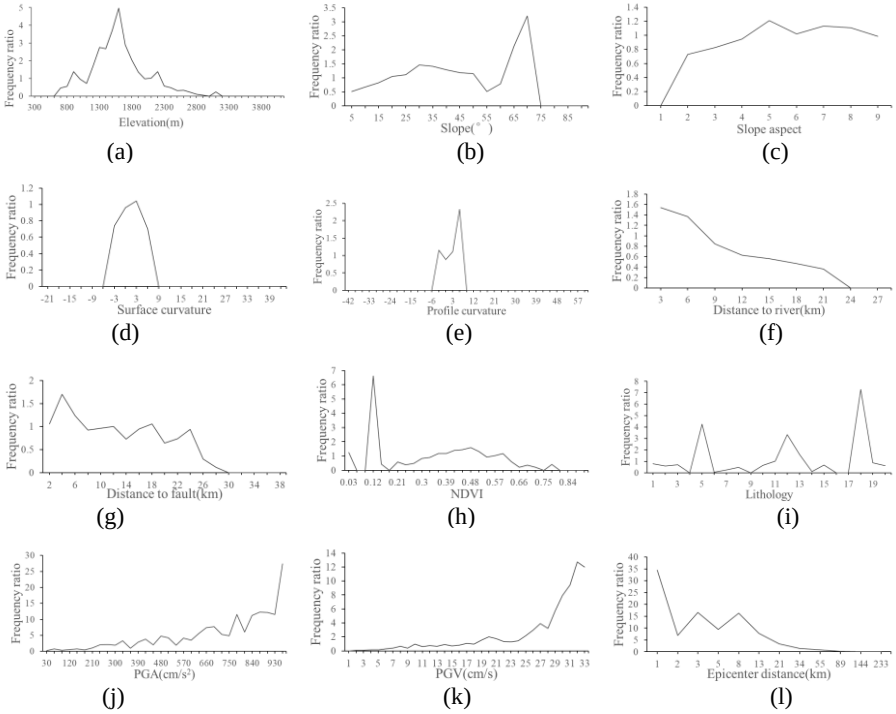

Fig. 6. Frequency ratio of various factors

3 Seismic landslide susceptibility analysis

3.1 Methodology

Landslide susceptibility analysis is able to evaluate the spatial probability of seismic landslide. The factor analysis reveals that the relation between factors and landslide susceptibility is characterized by high dimensions and nonlinear properties. In this study, two non-deterministic methods including BP neural network and support vector machine are used to analyze the susceptibility of seismic landslides, and the accuracy of the assessment results of the models is compared.

3.1.1 BP neural network

BP neural network is a feedforward multilayer network model, which can establish any nonlinear mapping from input to output. Data is transmitted forward from input layer to output layer, and the error between the calculated data and the real data is fed back from the output layer to the input layer. The structure of a simple BP neural network can be divided into input layer, hidden layer and output layer, as shown in Fig. 7. The mapping relation between input and output is established with the activation function and threshold in hidden layer. A classical three-layer network including one hidden layer is adopted. Except for the output layer, each layer could have differ-

ent numbers of neurons. The neuron number of input layer corresponds to the number of influencing factors, and the neuron number of hidden layer would be optimized based on the error of testing set. The network building process is composed of three steps, including forward calculation, error back propagation and weight update.

3.1.2 SVM

SVM (support vector machine) is a commonly used machine learning algorithm following the principle of structural rick minimization. It has been widely applied in decision making and data forecasting of various fields. The two fundamental components of SVM are the kernel function and the optimal classification hyperplane (Fig. 8). The kernel function could transform the input data into high dimensional space, to separate the data linearly. The commonly used kernel functions include linear kernel function, polynomial kernel function, radial basis function and sigmoid kernel function. Radial basis function is selected as the kernel function in the present research. And the hyperplane helps to discrete the input samples in the high dimensional space and maximize the classification margin between hyperplane and vector samples.

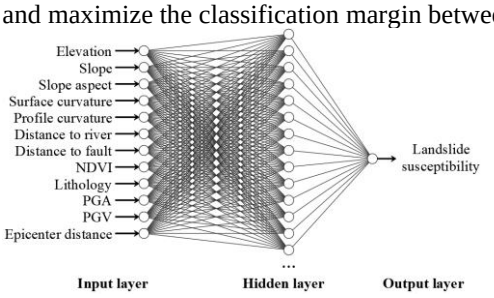

Fig. 7. BP neural network structure diagram

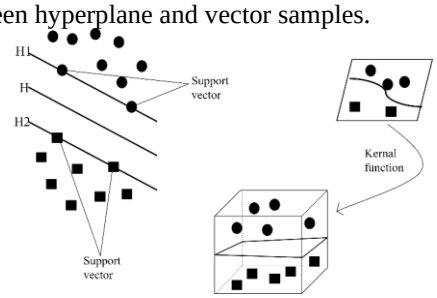

Fig. 8. Basic principles of SVM

3.2 Seismic landslide susceptibility result

70% of all samples constitute the test set and the rest 30% are categorized into verification set for network training. The label value of landslide data and non-landslide data are set as 1 and -1, respectively. And 0 is determined as the label value threshold to distinguish the category of landslide and non-landslide. The label value of susceptibility results greater than 0 is classified as landslide.

The comparison between actual landslide inventory and susceptibility results from different methods is shown in Fig. 9. It can be found that two machine learning algorithms produce relatively good susceptibility map with smooth transition of landslide among hilly area. Compared to the actual landslide points from inventory map, the results of BP neural network show fewer landslides, which are concentrating in the area near the epicenter. However, in the actual situation, there are some landslides occurred far from the epicenter. The results of BP neural network show dependency on spatial distribution of seismic ground motion parameters like PGA, PGV, and epicenter distance. The results of SVM show more discrete evaluation results of seismic landslide susceptibility. Some regions far from epicenter also have landslide area, which shows consistence with the actual distribution of seismic landslides.

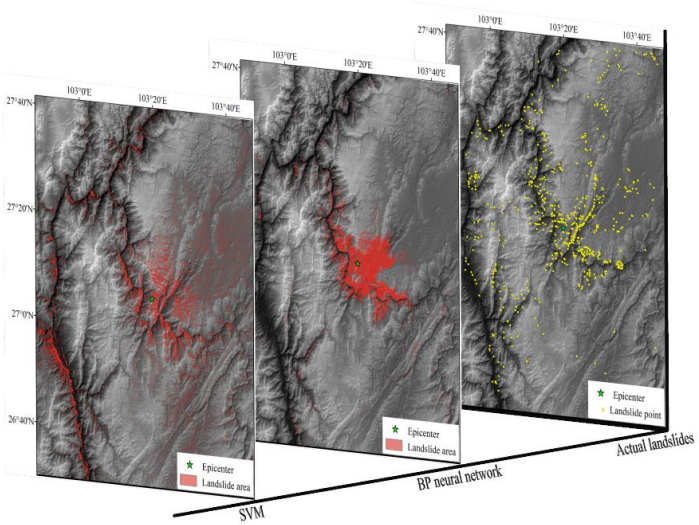

Fig. 9. Seismic landslide susceptibility map

To quantitively assess the performance of two machine learning algorithms, the Receiver Operating Characteristic (ROC) curve is adopted. The closer the curve is to the upper left corner of the coordinate system, the higher the proportion of landslide judged as positive results, indicating that the evaluation result of the model is more accurate. The area under the curve is defined as AUC (area under curve) value, which can be used to quantitatively compare the accuracy. The ROC curves of BP neural network and SVM are shown in the Fig. 10. The AUC values of two curves are 90.1% and 89.5%, respectively, showing that BP neural network has higher accuracy of seismic landslide susceptibility results. It can be observed that although the distribution trend of SVM result is similar to the actual landslide points, a large number of non-landslide points are evaluated as landslide points, greatly increasing the number of landslide points and reducing the accuracy. In addition, rainfall could be an important factor related to the seismic landslide susceptibility under Ludian earthquake. Ignoring the presence of rainfall factor might decrease the accuracy of results.

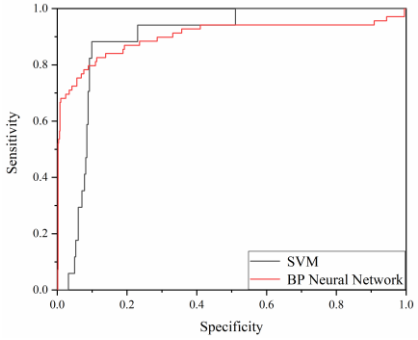

Fig. 10. ROC curves of SVM and BP neural network

4 Discussion

4.1 Comparation with Yangbi earthquake in typical ground motion

On May 21, 2021, a Ms 6.4 earthquake occurred in Yangbi County, Yunnan Province. The magnitude with 0.1 smaller than Ludian earthquake, but the disaster shows big difference. Few landslides occurred in Yangbi earthquake.

53YBX station with epicentral distance 8.6km shows that the PGA in three directions is 379.8cm/s^2, 720.3cm/s^2 and 448.4cm/s^2 respectively, as shown in Fig. 11 and the corresponding duration (Kawashinat bracketed duration with ratio 0.3) is 4.9s, 2.1s and 5.1s. Marginal spectrum of the station is shown in Fig. 12. Compared with 53LLT in Ludian earthquake, cumulative energy is evenly distributed in high (10-15Hz) and low frequency (approximately 2Hz) and the energy of high frequency in NS direction is larger than low frequency. The results are corresponding to the theory that high frequency seismic ground motion with shorter wavelength than dimensions of slopes unlikely trigger landslides and low frequency seismic wave with longer wave-length than dimensions of slopes can lead slope move in the same direction, which more likely induce landslides [37-38].

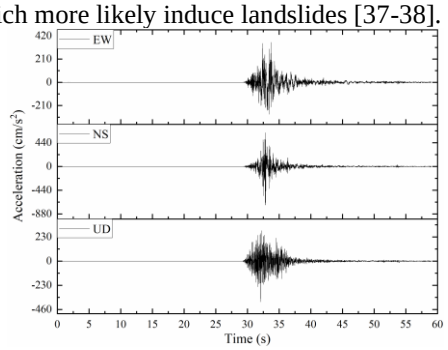

Fig. 11. Acceleration time history of 53YBX

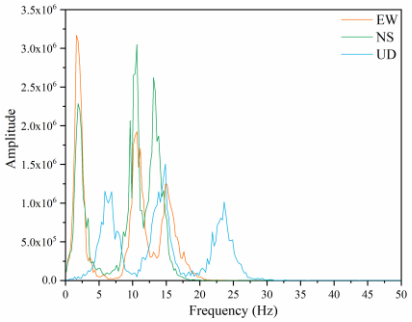

Fig. 12. Marginal spectrum of 53YBX

4.2 Landslide susceptibility evaluation considering characteristics of ground motion

This work indicates that the size and the number of landslides is closely related to the characteristics of ground motion especially in frequency domain. However, landslide susceptibility evaluation methods at present only take PGA or PGV into consideration to reflect the effect of earthquake. Obviously, the evaluation result is inconsistent with the actual situation. So, it is need to develop a susceptibility evaluation method that can reflect the frequency characteristics of seismic ground motion, which can improve the accuracy of evaluation result and have meaningful guiding significance for disaster prevention and reduction planning.

5 Conclusion

1. Ground motion in the epicenter of Ludian earthquake shows special characteristics. In time domain, PGA in EW direction up to 949.2cm/s^2, and the corresponding duration is 5.0s which show short duration characteristic. In time-frequency domain, large instantaneous and cumulative energy based on Hilbert spectrum and marginal spectrum respectively concentrate in low frequency region (0-5Hz), which easily trigger large landslides.

2. Approximately 720 landslides or rockfalls distribute within 60km of the epicenter of Ludian earthquake, with sliding distance ranges from 20 to 850m. The distribution of landslides influenced by elevation, slope, slope aspect, curvature, river, NDVI, PGA and PGV and Lithology. Among them, landslide sensitivity shows a good relationship with the increase of PGA and PGV and the decrease of epicenter distance, and the sensitivity reaches the largest in the class with the largest PGA and PGV and the class closest to the epicenter.

3. Seismic landslide susceptibility method based on machine learning (BP neural network and SVM) can well determine the distribution of landslides. The actual distribution of landslides is closer to the result of SVM. However, the BP neural network has higher accuracy than SVM. This is because that a large number of non-landslide points are determined as landslide points by SVM.

Acknowledgments:

This work is financially supported by the National Key R&D Program of China (2018YFC1504504).

References

1. Huang R, Fan X. The landslide story. Nature Geoscience, 2013, 6(5): 325-326.
2. Calais E, Minster J B. GPS detection of ionospheric perturbations following the January 17, 1994, Northridge Earthquake. Geophysical Research Letters, 2013, 22(9): 1045-1048.
3. Aydan Ö. Some considerations on a large landslide at the left bank of the Aratozawa dam caused by the 2008 Iwate–Miyagi intraplate earthquake. Rock Mechanics and Rock Engineering, 2016, 49(6): 2525-2539.
4. Moratto L, Vuan A, Saraò A. A hybrid approach for broadband simulations of strong ground motion: the case of the 2008 Iwate–Miyagi Nairiku earthquake. Bulletin of the Seismological Society of America, 2015, 105(5): 2823-2829.
5. Lai J, He S, Qiu J, Chen J, Wang L, Wang K, Wang J. Characteristics of seismic disasters and aseismic measures of tunnels in Wenchuan earthquake. Environmental Earth Sciences, 2017, 76(2): 1-19.
6. Guo X, Peng C, Li Y, Zou Q, Kong Y. The formation and development of debris flows in large watersheds after the 2008 Wenchuan Earthquake. Landslides, 2016, 13(1): 25-37.
7. Zhang Y, Zhang J, Chen G, Zheng L, Li Y. Effects of vertical seismic force on initiation of the Daguangbao landslide induced by the 2008 Wenchuan earthquake. Soil Dynamics & Earthquake Engineering, 2015, 73: 91-102.

8. Chen Q, Cheng H, Yang Y, Liu G X, Liu L Y. Quantification of mass wasting volume associated with the giant landslide Daguangbao induced by the 2008 Wenchuan earthquake from persistent scatterer In-SAR. Remote Sensing of Environment, 2014, 152: 125-135.
9. Yang C, Liu X, Zhang J. Analysis on mechanism of landslides under ground shaking: a typical landslide in the Wenchuan earthquake. Environmental Earth Sciences, 2014, 72(9): 3457-3466.
10. Yamagishi H, Yamazaki F. Landslides by the 2018 Hokkaido Iburi-Tobu Earthquake on September 6th. Landslides, 2018, 15: 2521-2524.
11. Trifunac MD. 75th anniversary of strong motion observation – a historical review. Soil Dyn Earthq Eng 2009;29(4):591–606.
12. Lu DW, Yang ZB. Strong Motion Observation from Recent Destructive Earthquakes in China Mainland. AMM 2015;724:358–61.
13. Wang DC, Ni SD, Li J. Research status of rapid assessment on seismic intensity. Progress in Geophys. (in Chinese), 2013, 28(4): 1772-1784.
14. Panzera F, Lombardo G, Imposa S, Grassi S, Gresta S, Catalano S, Romagnoli G, Tortorici G, Patti F, Di Maio E (2018) Correlation between earthquake damage and seismic site efects: the study case of Lentini and Carlentini, Italy. Eng Geol 240:149–162.
15. Jia H, Chen F, Pan D (2016) Comparison of two large earthquakes in China: the Ms 6.6 Yunnan Jinggu Earthquake and the Ms 6.5 Yunnan Ludian Earthquake in 2014. Int J Disaster Risk Reduct 16:99–107.
16. Bozzano, F., Lenti, L., Martino, S., Paciello, A., and Scarascia Mugnozza, G.: Self-excitation process due to local seismic amplification responsible for the 31st October 2002 reactivation of the Salcito landslide (Italy), J. Geophys. Res., 113, B10312, 2008.
17. Bozzano, F., Lenti, L., Martino, S., Montagna, A., and Paciello, A.: Earthquake triggering of landslides in highly jointed rock masses: Reconstruction of the 1783 Scilla rock avalanche (Italy), Geomorphology, 129, 294–308, 2011a.
18. Bozzano, F., Lenti, L., Martino, S., Paciello, A., and Scarascia Mugnozza, G.: Evidences of landslide earthquake triggering due to self-excitation process, Int. J. Earth Sci., 100, 861–879, 2011b.
19. Del Gaudio, V. and Wasowski, J.: Advances and problems in understanding the seismic response of potentially unstable slopes, Eng. Geol., 122, 73–83, 2010.
20. Lenti, L. and Martino, S.: The interaction of seismic waves with step-like slopes and its influence on landslide movements, Eng. Geol., 126, 19–36, 2011.
21. Martino, S. and Scarascia Mugnozza, G.: The role of the seismic trigger in the Calitri landslide (Italy): historical reconstruction and dynamic analysis, Soil Dynam. Earthq. Eng., 25, 933–950, 2005.
22. Kramer S L, Smith M W. et al. (1997). Modified Newmark Model for Seismic Displacements of Compliant Slopes[J]. Journal of Geotechnical and Geoenvironmental Engineering, 123(7): 635-644.
23. Randall W. Jibson, Hakan Tanyaş. (2020). The influence of frequency and duration of seismic ground motion on the size of triggered landslides—A regional view, Engineering Geology, Volume 273, 105671.
24. Baker JW, Cornell CA. Vector-valued intensity measures for pulse-like near-fault ground motions. Eng Struct 2008;30(4):1048–57.
25. Iervolino I, Chioccarelli E, Baltzopoulos G. Inelastic displacement ratio of nearsource pulse-like ground motions. Earthq Eng Struct Dyn 2012;41(15):2351–7.
26. Shinoda M, Miyata Y. Regional landslide susceptibility following the Mid NIIGATA prefecture earthquake in 2004 with NEWMARK'S sliding block analysis. Landslides, 2017, 14(6): 1887-1899.

27. Chen X, Shan X, Wang M, et al. Distribution pattern of coseismic landslides triggered by the 2017 Jiuzhaigou Ms 7.0 earthquake of China: control of seismic landslide susceptibility. ISPRS International Journal of Geo-Information, 2020, 9(4): 198.
28. Huang D, Wang G, Du C, et al. An integrated SEM-Newmark model for physics-based regional coseismic landslide assessment. Soil Dynamics and Earthquake Engineering, 2020, 132: 106066.
29. Han L, Ma Q, Zhang F, et al. Risk assessment of an earthquake-collapse-landslide disaster chain by Bayesian network and Newmark models. International journal of environmental research and public health, 2019, 16(18): 3330.
30. Wang Y, Song C, Lin Q, et al. Occurrence probability assessment of earthquake-triggered landslides with Newmark displacement values and logistic regression: The Wenchuan earthquake, China. Geomorphology, 2016, 258: 108-119.
31. Huang Y, Zhao L. Review on landslide susceptibility mapping using support vector machines. Catena, 2018, 165: 520-529.
32. Hong H, Pradhan B, Bui D T, et al. Comparison of four kernel functions used in support vector machines for landslide susceptibility mapping: a case study at Suichuan area (China). Geomatics, Natural Hazards and Risk, 2017, 8(2): 544-569.
33. Shahri A A, Spross J, Johansson F, et al. Landslide susceptibility hazard map in southwest Sweden using artificial neural network. Catena, 2019, 183: 104225.
34. Xi W, Li G, Moayedi H, et al. A particle-based optimization of artificial neural network for earthquake-induced landslide assessment in Ludian county, China. Geomatics, Natural Hazards and Risk, 2019, 10(1): 1750-1771.
35. Moayedi H, Mehrabi M, Kalantar B, et al. Novel hybrids of adaptive neuro-fuzzy inference system (ANFIS) with several metaheuristic algorithms for spatial susceptibility assessment of seismic-induced landslide. Geomatics, Natural Hazards and Risk, 2019, 10(1): 1879-1911.
36. Hong H, Liu J, Zhu A X, et al. A novel hybrid integration model using support vector machines and random subspace for weather-triggered landslide susceptibility assessment in the Wuning area (China). Environmental Earth Sciences, 2017, 76(19): 1-19.
37. Shahri A A, Moud F M. Landslide susceptibility mapping using hybridized block modular intelligence model. Bulletin of engineering geology and the environment, 2021, 80(1): 267-284.
38. Dou J, Yunus A P, Merghadi A, et al. A Comparative Study of Deep Learning and Conventional Neural Network for Evaluating Landslide Susceptibility Using Landslide Initiation Zones//Workshop on World Landslide Forum. Springer, Cham, 2020: 215-223.
39. Polykretis C, Chalkias C. Comparison and evaluation of landslide susceptibility maps obtained from weight of evidence, logistic regression, and artificial neural network models. Natural hazards, 2018, 93(1): 249-274.
40. Sadighi M, Motamedvaziri B, Ahmadi H, et al. Assessing landslide susceptibility using machine learning models: a comparison between ANN, ANFIS, and ANFIS-ICA. Environmental Earth Sciences, 2020, 79(24): 1-14.